CFD-BASED FAN OPTIMIZATION CONSIDERING THE SYSTEM INTEGRATION IN A HEAT PUMP

Frieder LÖRCHER

ZIEHL-ABEGG SE, Ventilation Division, Heinz-Ziehl-Strasse, 74653 Künzelsau, Germany

SUMMARY

A fan is designed for a typical annual operation cycle for a heat pump concept. Four representative operating points have been defined with attributed numbers of operating hours per year. The design of the fan is based on CFD simulations of the entire airside of the heat pump. The properties of the heat exchanger (HEX) under different operating conditions (pressure drop and heat transfer) are modelled locally on the HEX based on experimental data. For each evaporator duty point, defined by the heat transfer power from air to HEX, the required rotation speed and electrical power input are computed with the generated model. The annual electrical power input is minimized within a semi-automatic optimization.

INTRODUCTION

Fan performance data, such as duty points, total-to-static efficiencies, total-to-total efficiencies or sound power levels obtained considering standard lab conditions may not contain sufficient information to determine the fan behavior incorporated in a higher level unit. In extreme cases, fans with high efficiencies and low noise emissions may show poor behavior under operating condition in a unit where they are installed. More generally spoken, a fan optimized under standard conditions, for example just considering a nominal duty point of the target unit, may differ considerably from a fan optimized under real operating condition in the target unit.

Installation effects already have been subject of many investigations in the past. In [1], installation effects for a fan have been investigated experimentally with the outcome, that the shift of load towards the blade tip makes the fan less sensitive to inflow disturbance. Response surfaces have been generated for a parametrization of fan supports, based on which optimization have been carried out. In [2], installation effects of an air cooled steam condenser with both one and three axial fans have been investigated, and the fans have been optimized with respect to the installation effects. In [3], a more general investigation of inlet installation effects on different types of fans is presented.

In the present paper, a fan optimization considering a particular heat pump unit is carried out. This work emerged in the context of the EU-funded research project “Next Generation Heat Pump for Retrofitting Buildings“ [4]. In this project, a consortium of research institutes and component

suppliers for heat pumps aims to conceive a 30 kW peak capacity heat pump for retrofitting buildings in urban areas. The main objectives for the fan and air-side development of the heat pump are the minimization of the power consumption of the fan, which has to assure the heat transfer to the evaporator HEX under any operating condition, and the minimization of fan noise generation.

HEAT PUMP FRAMEWORK

Geometrical framework of the heat pump

The geometrical framework conditions of the heat pump have been fixed as outlined in *Figure 1*. The HEX is positioned horizontally, and the main airflow direction through the heat pump is from bottom to top. The main reasons for this arrangement come from icing and defrosting considerations. The fan is sucking air from the HEX. Pushing air over the HEX was considered in an earlier phase, but a high risk of thermal shortcuts was identified, which is avoided by "throwing" the down-cooled air with high exit velocity downstream of the fan to the adjacent space.

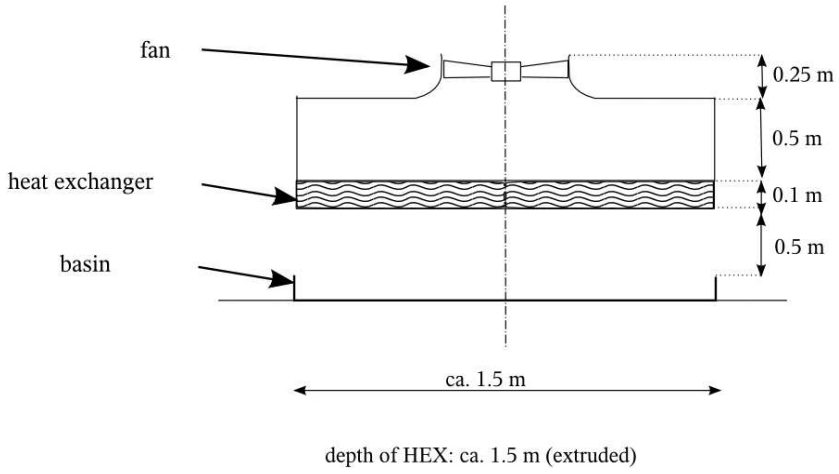

Figure 1: Geometrical outline of the heat pump

The inflow/outflow surfaces of the HEX are approximatively square shaped with length $L_{HEX} = 1.5\,m$ and width $B_{HEX} = 1.5\,m$. The depth in airflow direction of the HEX is $D_{HEX} = 0.1\,m$, and the distance fan inlet plate – HEX is $0.5\,m$. The HEX is elevated about $0.5\,m$ over the floor. This gives sufficient area for laterally inflowing air.

Design operation point (full capacity)

At full capacity operation, the heat transfer required from air to the HEX is $Q_{des} = 18.4\,kW$. The difference between the temperature of inflowing air and the evaporation temperature of the coolant (Propane) is $T_{air,in} - T_{coolant,evap} = 7\,K$. For the present work, the temperature of the HEX is approximated to be constant. As superheating is applied in the evaporator, the temperature of the HEX is supposed to be about $1.2\,K$ higher than the coolant evaporation temperature and thus $5.8\,K$ lower than the incoming air temperature: $T_{air,in} - T_{HEX} = T_{air,in} - \left(T_{coolant,evap} + 1.2\,K\right) = 5.8\,K$.

From the HEX dimensioning, at dry condition, an air volume flow rate of $\dot{V}_{des} = 2.8\frac{m^3}{s}$ at design air density of $\rho = 1.33\frac{kg}{m^3}$ was supposed to be required in order to achieve the required heat transfer.

This information is used in Section *Validation of heat transfer model* to verify the CFD heat transfer model at dry design condition. With definition of the superficial velocity u_{sup} on the HEX given by

$$u_{sup} = \frac{\dot{V}}{A_{HEX}} \quad (1),$$

where $\dot{V}$ is the air volume flow rate and $A_{HEX} = L_{HEX} \cdot B_{HEX}$, the design superficial velocity on the HEX is $u_{sup,des} = \frac{\dot{V}_{des}}{A_{HEX}} = 1.244 \frac{m}{s}$.

Pressure loss of the HEX and its modelling

For the CFD simulations, the HEX is not resolved in detail, but modelled as porous medium. The properties of this medium concerning pressure loss depend strongly on the actual icing condition. In order to define them, experimental data is incorporated. In *Figure 2*, the HEX pressure loss is shown as function of the superficial velocity for dry condition, medium icing condition (after $15\,min$ icing progression), and max icing condition (after $30\,min$ icing progression). For modelling purposes, the experimental data is approximated by polynomials with linear coefficients C_1 and quadratic coefficients C_2. The design superficial velocity $u_{sup,des} = 1.244 \frac{m}{s}$ induces, at dry condition, the design pressure loss $\left(\frac{\Delta p}{\rho}\right)_{des} = 13 \frac{m^2}{s^2}$, which is comparatively low. The pressure loss coefficients of the HEX are summarized in *Table 1*.

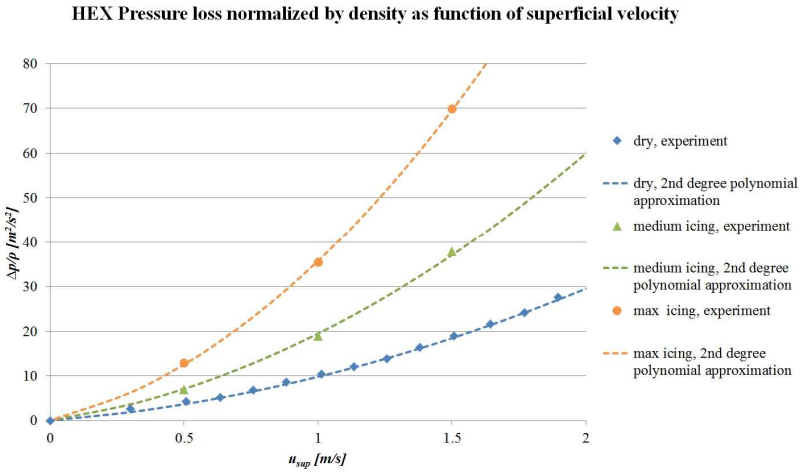

Figure 2: HEX pressure loss as function of the superficial velocity

Table 1: Pressure loss coefficients under different icing conditions

	C1 [m/s]	***C2 []***
dry	*4.859*	*4.954*
medium icing	*8.981*	*10.491*
max icing	*14.525*	*21.241*

In the CFD simulations, the HEX region is modelled as porous medium. Linear and Quadratic streamwise pressure loss coefficients are prescribed in accordance to *Table 1*. Transverse losses are prescribed to be higher by a factor of *10* .

Heat transfer to the HEX and its modelling

The heat transfer to the HEX is modelled as function of the superficial velocity distribution on the HEX outlet surface solely. The heat transfer ∂Q normalized by the HEX outlet area and the difference between HEX temperature and locally averaged air temperature given by

$$T_{air,ave} = T_{HEX} + \left(\frac{2\rho \cdot c_{p,air} \cdot u_{\sup}}{2\rho \cdot c_{p,air} \cdot u_{\sup} + \partial Q} \right) \cdot \left(T_{air,in} - T_{HEX} \right) \qquad (2)$$

is modelled by the Reynolds-exponent-approach

$$\partial Q = X \cdot \left(Re\left(u_{sup,}, D_{HEX}, \nu_{air} \right) / Re_0 \right)^m \qquad (3)$$

where X is a heat transfer coefficient, $Re_0 = 8000$ a reference Reynolds number and m a Reynolds number exponent. By adjustment to experimental data, the values given in *Table 2* have been derived.

Table 2: Coefficients for the computation of the heat transfer

	$X\left[kW/\left(K \cdot m^2\right)\right]$	**exponent *m* []**
dry	*1.900*	*0.51*
medium icing	*1.773*	*0.47*
max icing	*1.639*	*0.41*

In *Figure 3*, a comparison of experimental data and the model output is presented for the dry condition.

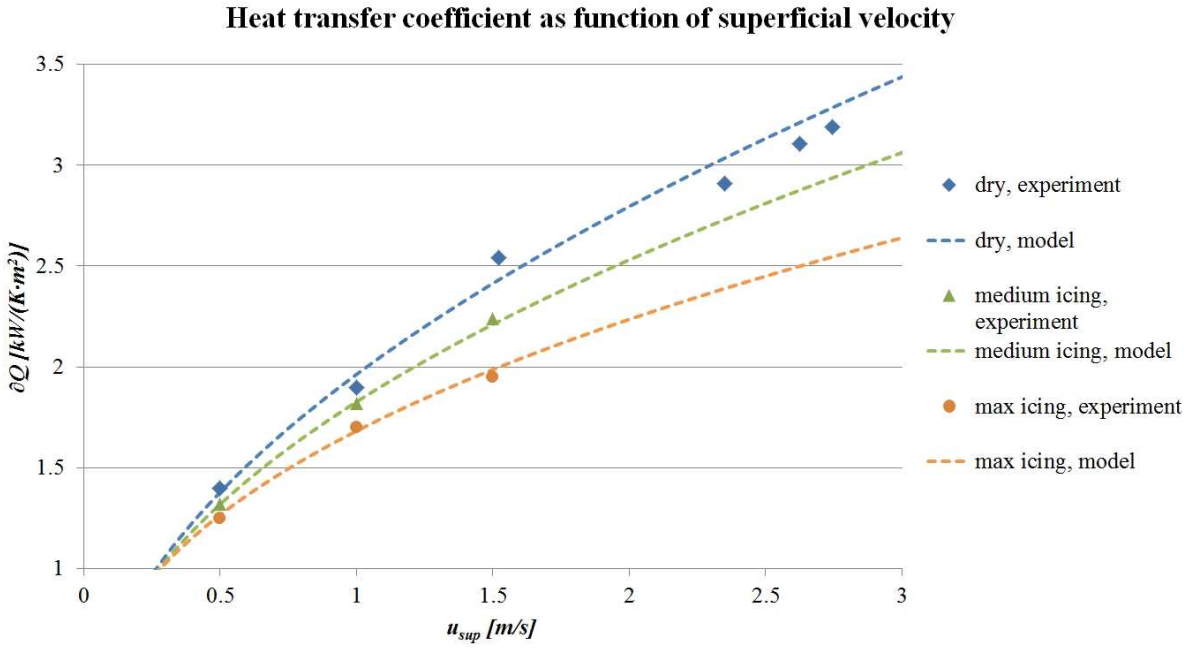

Figure 3: Heat transfer coefficient ∂Q as function of the superficial velocity u_{sup} under dry and icing conditions

With given velocity distribution from a CFD simulation, the distribution of ∂Q can be computed with Equation (3) and the coefficients of *Table 2*. Using Equation (2), the total heat transfer then can be evaluated with the surface integral

$$Q = \int_{HEX\_Outlet} \partial Q \cdot \left(T_{air,ave} - T_{HEX} \right) dA \qquad (4).$$

Electric motor and its modelling

A given electrical motor was incorporated to the fan optimization. A comparatively small EC (electronically commuted)-motor of diameter $0.09\,m$ (at the air gap) is used. The advantages of this smaller motor in the greenHP unit are the low weight, the low investment, the reduced use of production resources (material and energy), even though bigger motors would have had a slightly higher efficiency. On the other hand, the smaller motor allows for a smaller hub-to-tip ratio of the fan, which is favorable for the fan efficiency at operating points with low pressure drops. However, the smaller motor shows significant sensitivity of its electric efficiency $\eta_{mot} = P_{shaft} / P_{electric}$, which is a function of the rotational speed and the shaft power. For this reason, we considered as optimization target the electrical power rather than the shaft power. This corresponds to the system idea of the present optimization work. The interface of the unit level to the component "fan" is on the input side the electrical power, on the output side the heat transfer on the HEX.

In *Figure 4*, experimental data of motor efficiency is shown as function of the shaft power for different rotation speeds. For the evaluation of the electrical power input, we interpolate in a linear way in this data with the shaft power and rotational speed given by a CFD-simulation result in order to approximate the motor efficiency and thus the electrical power. We note that the considered motor and the frequency inverter are one integrated unit, meaning also that the inverter efficiency is already incorporated within the motor efficiency.

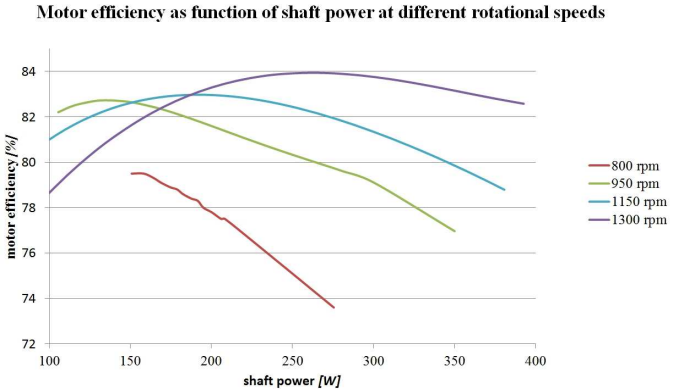

Figure 4: Motor efficiency curves for different rotational speeds

Time line of required evaporator capacity and definition of representative operation points

In *Figure 5*, the time line of the required evaporator charge is presented as factor relative to the design capacity of $P_{HEX,des} = 18.4\,kW$. The time resolution of the data is $3\,min$. Below a required value of 0.6, on-off cycles are preferred. The complex devolution of the required capacity is simplified in an energy-conservative way and we define the representation of this time line by 2 capacity points: $P_{HEX,des} = 18.4\,kW$ and $P_{HEX,part} = 0.6 \cdot 18.4\,kW = 11.04\,kW$, where, over 1 year, the first (full capacity) point has to run $3955\,h$ and thus to bring $61110\,kWh$, and the second, part capacity point has to run $2334\,h$ and bring thus $25207\,kWh$. The occurrence of icing has important impact only for the full capacity point, which is therefore subdivided in three different representative operating points: dry, medium icing, and max icing. A summary of the representative operation points considered and their annual runtime according to data from the greenHP project is given in *Table 3*.

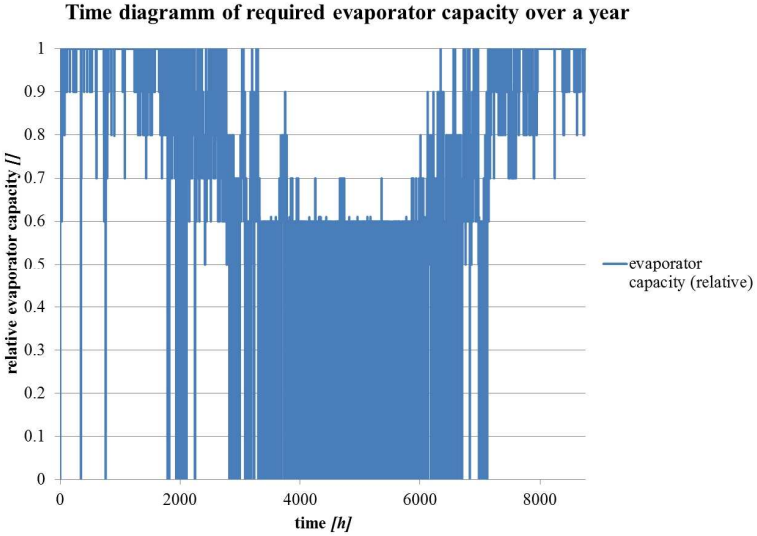

Figure 5: Time line of the required evaporator capacity over a year

Table 3: Representative operation points and their required runtime

	heat power Q *[kW]*	**icing state**	**annual runtime *[h]***	**annual heat transfer *[kWh]***	**air density** $\left[\frac{kg}{m^3}\right]$
OP 1	*18.4*	dry	*1425*	*25650*	*1.3*
OP 2	*18.4*	medium	*1062*	*19116*	*1.33*
OP 3	*18.4*	max	*908*	*16344*	*1.33*
OP 4	*11.04*	dry	*2334*	*25207*	*1.2*

SET UP OF A FAN BLADE GEOMETRY (GEOMETRY PARAMETERS)

Construction of axial fan blade geometry using sections

The construction principle of fan blades used in the present work is it to define n_{sec} blade sections at different radii $R_i, i = 1 \ldots n_{\text{sec}}$. The blade surfaces (suction side, pressure side, leading edge region and trailing edge region) are then built by construction of spline surfaces containing the curves of the different sections. In the left sketch of *Figure 6*, this is illustrated by an example using $n_{\text{sec}} = 5$ sections at the radii R_1 - R_5. In the present fan design, we use $n_{\text{sec}} = 5$ sections at fixed radii R_i defined as

$$R_i = R_1 + (R_{n_{\text{sec}}} - R_1)\frac{1 - \cos\left(\frac{i-1}{4}\pi\right)}{2} \qquad (5),$$

leading to a concentration of sections in the hub and the tip regions, being crucial regions for optimal fan design.

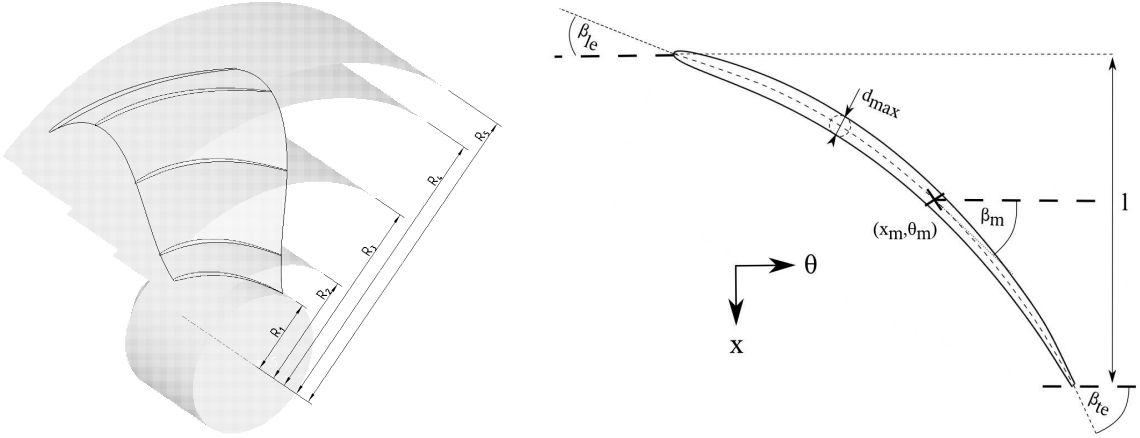

Figure 6: Example of a fan blade construction using section curves (right) at different radii R_1 - R_5 (left)

Definition of blade sections

Each section is defined using the method illustrated in right sketch of *Figure 6*, which is a plane (uncoiled) presentation of a section at $R_i = const$. The coordinate x represents the direction of the main flow (parallel to the fan axis), and the coordinate θ represents the circumferential direction (direction of rotational speed). The geometry of each section is built in two steps: First, the centerline (dashed) is constructed, and second, a thickness distribution is superimposed to the centerline to get a blade with finite thickness. The centerline is parametrized by its axial and

circumferential positions x_m and θ_m, its axial extension l, the leading edge angle β_{le}, the trailing edge angle β_{te} and the angle β_m at intermediate axial extension. The stacking is controlled by the radial distribution of x_m and θ_m for the different sections. For each section, the thickness distribution $d(\sigma)$, where σ is the normalized centerline position, is computed based on the basis thickness distribution $d_{Basis}(\sigma)$ shown in *Figure 7* using the formula $d(\sigma)=\left(F_1\cdot(1-\sigma)+F_2\cdot\sigma\right)\cdot d_{Basis}(\sigma)$. With the factors F_1 and F_2, the thickness in the front and trailing edge regions, respectively, are controlled. The choice of the factors F_1 and F_2 depended in the present work mainly on stability and manufacturing issues, as it turned out, that profiles with minimal possible thicknesses, especially at the trailing edges, lead to the best results.

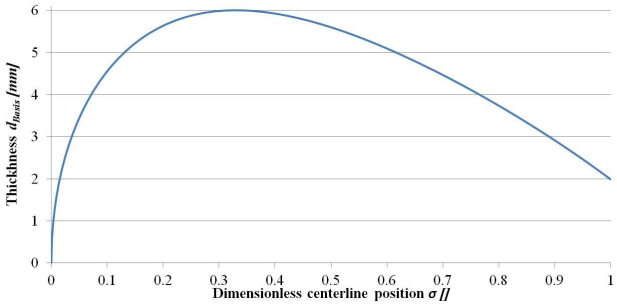

Figure 7: Basis thickness distribution for blade sections based on NACA 4 digit airfoils

Number of free parameters with respect to optimization

The outer sidewall contour is chosen out of 4 available inlet nozzles in norm diameters (0.*56 m*, 0.*63 m*, 0.*71 m* and 0.*80 m*). The tip gap is determined by tolerance considerations solely, thus the impeller diameter (corresponds to R_5) has *4* discrete possible values. The hub diameter (corresponds to R_1) is fixed to the outer diameter of the pre-selected external rotor motor. The number of blades is an additional free parameter. However, it is our best practice to avoid the blade numbers *2*, *4*, and *8* in order to reduce tonal noise components. Thus the blade number n_{blades} is chosen to be one of the discrete values *3*, *5*, *6*, *7* or *9* (higher blade numbers are not considered). This means, we end up with *31* free parameters for the optimization: for each of the *5* sections x_m, θ_m, l, β_{le}, β_{te} and β_m (unless θ_m of the first section, which is fixed to zero), R_5 and n_{blades}. *Two* of the free parameters, R_5 and n_{blades}, are limited to some discrete values.

Considering automatic optimization, the number of *31* free parameters is high. Automatic optimization of fans is subject of recent research work. In [5], an automatic optimization of swept axial fan blades, using the Nelder-Meat-method, based on RANS simulations, is presented. In the book of Thévenin [6], CFD based optimization is addressed which mainly refers to simplex, evolutionary or adjoint methods. In [7], an optimization methodology based on inverse design, CFD and a response surface method for fans was presented. In [8], the optimization of axial fans based on meta-models is discussed.

It is not the objective of this work to apply an automatic optimization algorithm. More emphasis is put on a parameter set being able to represent efficient fan design, therefore not limiting too much the number of parameters. Automatic optimization algorithms remain still very expensive in terms of computation time in order to resolve realistic fan optimization problems and obtain competitive solutions with competitive effort. Instead, a “semi-automatic” optimization is carried out, meaning, that everything (geometry construction, meshing, CFD setup, CFD solution and a sophisticated post-processing) is carried out automatically unless the closure of the optimization process between CFD results and choice of the parameter set for one or several new candidate geometries, which is done manually.

SETUP OF THE CFD SIMULATION

Geometrical domain, domain decomposition and mesh discretization

In *Figure 8*, a scheme of the domain decomposition of the entire fluid volume discretized within the CFD simulation (*left*) and a corresponding computational mesh (*right*) are shown. The non-rotating fluid domain "inlet domain" is a half-sphere with a circumferential extent of *360°*. At the inlet boundary, the mass flow is prescribed with velocity normal to the boundary surface. The "HEX domain" is a porous domain with the real exterior shape of the heat exchanger. The volume porosity (portion of fluid volume) is *0.75*, which is in good agreement to the real HEX. Linear and quadratic pressure loss coefficients are prescribed as described in Section *Pressure loss of the HEX and its modelling*. The non-rotating fluid domain "interior domain" is a complete discretization of the inner air volume of the evaporator which is basically a region with reduced pressure. The "rotor domain" is a rotating fluid domain enclosing the fan blade geometry. Only one blade is discretized and cyclic boundary conditions are applied in the "rotor domain" and the "outlet domain". The interfaces "interior domain" to "rotor domain" and "rotor domain" to "outlet domain" are modelled by mixing planes. The stationary "outlet domain" basically has the shape of a cylinder section. At the outlet boundary, an opening boundary condition is used, prescribing the static pressure in case of outflowing fluid and total pressure in the case of inflowing fluid.

The "HEX domain" is discretized by a structured hexahedral mesh with *32000* elements. The other domains are discretized by unstructured tetrahedron meshes with *8* prism boundary layers in the wall regions. A *Y+* value of the thickness of the first prism layer of *10-25* was realized. The overall mesh contains about *0.5-0.7 million* elements depending on the fan blade geometry. The intent was it to choose the number of mesh elements not too high in order to get quick response times for the simulations.

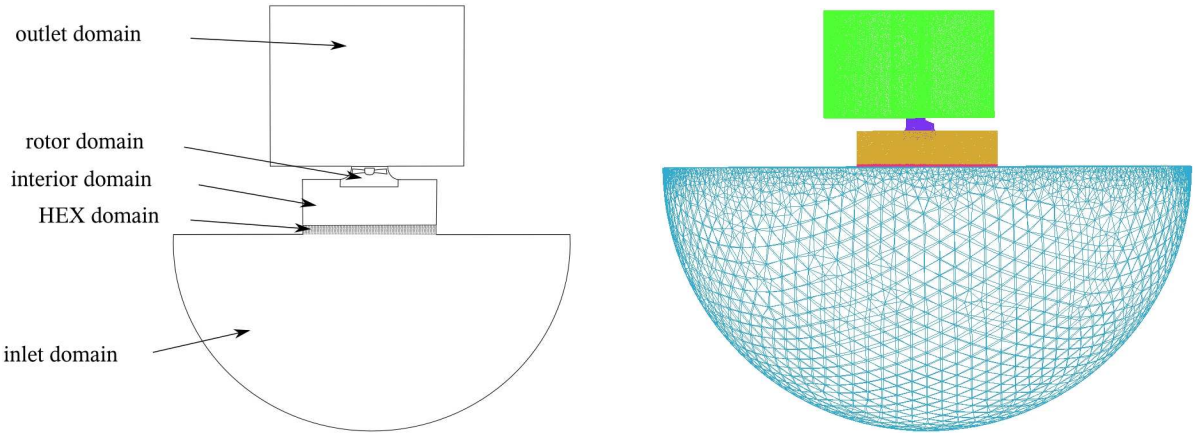

Figure 8: Scheme of the geometrical domains used in the CFD simulations (left) and computational mesh (right)

Setup of the computation for the simulation of one operation point

Incompressible simulations have been carried with air data for given fixed density chosen according to *Table 3*. The simulations were stationary RANS simulations. As turbulence model, the 2-equation SST-model (e.g. [9]) was used, and wall functions have been applied. At the inlet, a turbulence intensity of *5%* was prescribed. The simulations were realized with ANSYS CFX 14.5. For one run, *16* cores have been used, which lead to a simulation wall-clock time for one operating point and one rotational speed of about *0.5 h*. In total, *32* cores have been used for the simulations, allowing for two simulations to run in parallel.

The fan rotational speed was adjusted automatically in order to get the required heat transfer. At a first step, a run for a rough estimation (taken from an earlier run of another blade geometry) of the

rotation speed u_1 was computed to convergence. In a second step, a rotation speed u_2 was used assuming a purely quadratic loss behavior of the unit and homogenous velocity distribution on the HEX:

$$u_2^{\,m} = u_1^{\,m} \cdot \frac{Q_{req}}{Q_1} \qquad (6),$$

where *m* is the Reynolds number exponent (*Table 2*), Q_{req} means the required heat transfer, and Q_1 the resulting volume flow of run 1. The convergence error after this step was always smaller than *0.5%* for the heat transfer *Q*. Nevertheless, we still scale the resulting velocity field by the factor $\left(\frac{Q_{req}}{Q_2}\right)^{\frac{1}{m}}$ for the evaluation of the heat transfer to the HEX, which is then evaluated as described in section *Heat transfer to the HEX and its modelling*. The other relevant quantities like shaft power are scaled with the corresponding scaling laws.

Summing up the annual electric fan energy consumption and optimization loop

In order to get an estimation for the electric energy consumed by the fan over one year, a simulation is carried out for each of the representative operating points (*Table 3*). The electric power consumption is estimated from the shaft power consumption using the motor model of section *Electric motor and its modelling*. For each of the representative operating point, then the annual energy consumption can be computed simply by multiplying the electric power consumption with the annual runtime given in *Table 3*. Summing up the energy consumption of the *4* representative operating points, we get an estimation of the total annual fan energy consumption. This annual fan energy consumption directly relates to the operation costs caused by the fan, thus its optimization is the operators direct interest. In the present model, under given framework conditions of heat pump and motor, the annual fan energy consumption is a functional of the fan geometry solely, which we optimize by a "semi-automatic" optimization. In *Figure 9*, the process of an optimization loop is summarized.

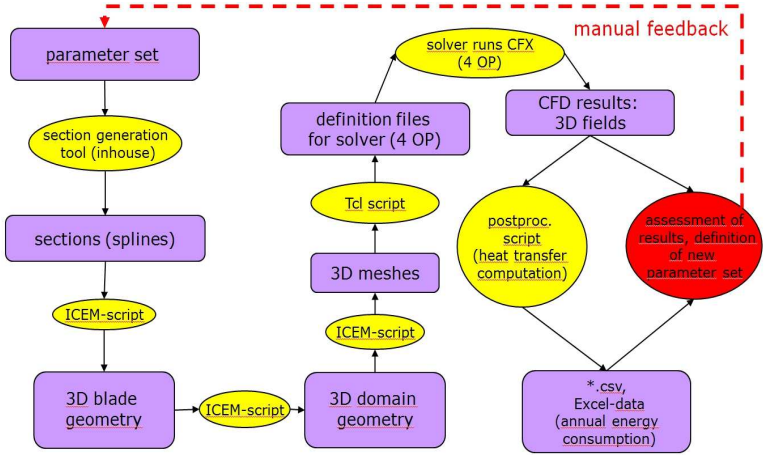

Figure 9: "Semi-automatic" optimization loop

RESULTS

Validation of heat transfer model

The HEX designers postulated at design condition a required air volume flow of $\dot{V}_{des} = 2.8\frac{m^3}{s}$ in order to obtain the design point heat transfer at dry condition of $Q_{design} = 18.4\,kW$. The required air volume flow of the favorite fan geometry at design condition was $\dot{V}_{req,des} = 2.97\frac{m^3}{s}$. This is slightly

higher than the prediction. But on the other hand, the prediction was computed assuming homogenous velocity distribution on the HEX. Non-homogenous velocity distributions lead to higher required air volume flows.

The best fan geometry found an its data

The best fan found within the present work (*Figure 10*, left) has a diameter of 0.*63 m* and has *3* blades, which are slightly forward swept. Its annual energy consumptions can be found in *Table 4*.

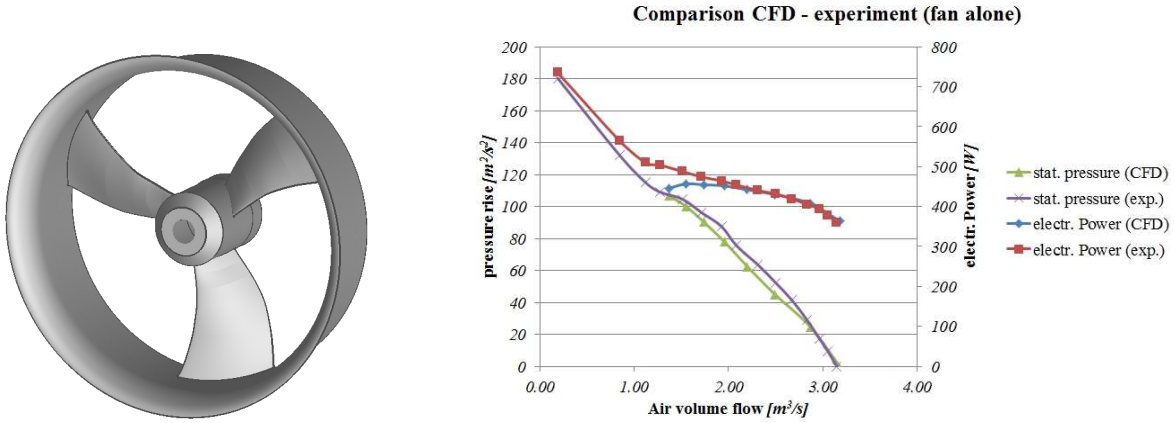

Figure 10: Best fan geometry / CAD view (left) and comparison CFD - experiment (right) at 1102 rpm

For comparison, the annual heat transfer onto the HEX is *86300 kWh*, which is nearly *42* times higher compared to the fan energy consumption of *2061 kWh*.

Comparisons CFD - experiment

A comparison of the CFD simulation of the fan alone in standard lab conditions (including the motor model) with the corresponding experiment at design point rotational speed of *1102 rpm* is shown in the right graph of *Figure 10*. The agreement is good in the relevant region of the air volume flow (in the diagram for $\dot{V} > 2.0 \frac{m^3}{s}$). Note that the diagram shows results for constant rotation speeds, whereas part load and icing situations of the heat pump are realized by varying the fan rotation speed.

Up to now, aerodynamic experiments with the HEX under dry conditions have been carried out. In the experiment, the required fan rotation speed in order to get the required dry condition air volume flow $\dot{V}_{req,des} = 2.97 \frac{m^3}{s}$ was *1107 rpm* compared to the *1102 rpm* in the simulation. The electrical power at this operating point in the experiment was *403 W* compared to the *400 W* in the simulation.

Discussion

- Concerning the fan diameter: for better velocity distribution on the HEX, being favorable both for high heat transfer at given volume flow and low pressure loss, bigger diameters are favorable. Concerning impeller efficiency in combination with motor efficiency (given motor), too big diameters lead to drawbacks. In sum, both the bigger fan diameter 0.*71 m* (sum of best fan *2440 kWh*) and the smaller fan diameter 0.*56 m* (sum of best fan *2770 kWh*) had significant inferior performance compared to the fan diameter 0.*63 m*.
- In *Table 4*, different fans designs are compared. These are the fans showing best performance each for one isolated duty point (considering only fans of diameter 0.*63 m*) Some of the fans go to stall, at least in CFD, in OP 3 (those with the question mark). For example, the fans “Best

OP 1" and "Best OP 4" are slightly backward leaned. The fan "best static efficiency" has quite radial geometry (no lean). The necessity of operating under the condition of OP 3 induces the fact that the blade is forward leaned, even though this leads to a deterioration of the efficiency over a large range. The main difference of the fans "Best OP 1" and "Best OP 4" is the power density. The "Best OP 4" fan has *7* blades and brings the design point at about *850 rpm*, whereas the "Best OP 1" fan has *3* blades and brings it at *1200 rpm*. However, the rotational speed has impact on the motor efficiencies. The impact of different fan geometries of the same diameter on the HEX velocity distributions was moderate. Concerning the actual ErP regulation rule, which considers the best static efficiency, one can clearly see, as we could have expected, that the best static efficiency may not be representative of a real unit's annual energy consumption.

Table 4: Comparison of best performance fans at isolated duty points

Annual cons. [kWh]	**SUM**	**OP 1**	**OP 2**	**OP 3**	**OP 4**
best fan	*2061*	*570*	*524*	*670*	*297*
best OP 1	*2256*	*544*	*522*	*890 (?)*	*290*
best OP 2	*2234*	*564*	*518*	*850 (?)*	*302*
best OP 3	*2087*	*599*	*525*	*655*	*308*
best OP 4	*2269*	*551*	*537*	*850 (?)*	*288*
best efficiency	*2282*	*555*	*520*	*915 (?)*	*292*

Note concerning the acoustically optimized final blade geometry

The fan blades resulting from the CFD optimization process with the given parametrization have been optimized subsequently for acoustical purposes. The fact that the blades are forward swept in the radially outward region is known to be favorable not only for the stall margin, but also from an acoustical point of view (see e.g. [5], [10], [11]). The blade tip regions are equipped with winglets (basically described e.g. in [12]), and the blade trailing edge is serrated in order to reduce trailing edge boundary layer noise, as is already proposed e.g. in [13].

CONCLUDING REMARKS

In order to optimize a fan for a given heat pump unit, a model was built up allowing it to analyze the annual electric energy consumption of a fan design as a part of the unit. A realistic duty profile of the heat pump including icing and part load situations has been considered. The fan rotational speed was at any time adjusted to ensure the desired heat transfer power from the air to the evaporator HEX. For that, the heat transfer was modelled, based on experimental data, as function of the velocity distribution on the HEX outlet.

The way in which the fan blade geometry was built up from a given parameter set was exposed. A tool was generated allowing it to get, starting from the parameter set for a fan blade, without manual intervention, the annual electric energy consumption as property of the fan geometry.

Using this tool, an optimization was carried out. The closure of the optimization loop between the simulation results and new parameter sets was done manually. Automatic optimization would lead to computational requirements beyond the author's possibilities. We were able to analyze over *100* fan geometries in this work.

Concerning the results, it was shown that the annual energy consumption can be reduced considerably compared to methods, where fans are selected just considering their best efficiency point or their efficiency at design duty point. Especially the high pressure drops under icing conditions have an important impact, even if they occur only in a smaller part of the operating time. These operating points lead to the necessity of a significantly forward swept blade.

ACKNOWLEDGEMENT

This work was supported within the project “Next generation Heat Pump for Retrofitting Buildings” supported by the EU.

BIBLIOGRAPHY

[1] E. Tannoury, B. Demory, M. Henner, P.-A. Bonnet, P. Caule, Y. Creteur – *A Design of Experiment of installation effects and the influence of blade loading on the aeroacoustics of an automotive Engine cooling fan.* Proceedings of Fan 2012 Symposium, Senlis, **2012**

[2] S.J. van der Spuy, T.W. von Backström, D.G. Kröger, P.R.P. Bruneau – *Testing an axial flow fan designed for air-cooled steam condenser application.* Proceedings of Fan 2012, Senlis, **2012**

[3] A. Guedel, B. Cory, M. Stevens – *Inlet installation effects on different types of fans and ductwork designs.* Proceedings of Fan 2012 Symposium, Senlis, **2012**

[4] M. Monsberger (project coordinator) – *Driving heat pump innovation through cutting edge research*. Newsletter, http://www.ehpa.org/about/media-library/newsletter/, **2012**

[5] K. Bamberger, T. Carolus – *Optimization of Axial Fans with highly swept blades with respect to losses and noise reduction.* Proceedings of Fan 2012 Symposium, Senlis, **2012**

[6] D. Thévenin, G. Janiga – *Optimization and Computational Fluid Dynamics*. Heidelberg: Springer Verlag GmbH, **2008**

[7] M. Zangeneh, M. de Maillard – *Optimization of fan noise by coupling 3D inverse design and automatic optimizer*. Proceedings of Fan 2012 Symposium, Senlis, **2012**

[8] K. Bamberger, T. Carolus – *Performance Prediction of Axial Fans by CFD-Trained Meta-Models*. ASME Turbo Expo 2014, Volume 1A: Aircraft Engine; Fans and Blowers, Düsseldorf, Germany, June 16–20, **2014**

[9] F. R. Menter – *Two-Equation Eddy-Viscosity Turbulence Models for Engineering Applications.* AIAA Journal, Vol. 32, No. 8 (1994), pp. 1598-1605, **1994**

[10] T. Carolus – *Sichelschaufeln bei Axialventilatoren*. VDI Bericht 1591(2001), S.443–457, **2001**

[11] T.B. Lindemann, J. Friedrichs, U. Stark – *Development of a New Design Method for High Efficiency Swept Low Pressure Axial Fans With Small Hub/Tip Ratio*. In: ASME Turbo Expo, June 16-204, **2014**

[12] W. Angelis, G. Eimer – *Einsatz von Winglets an Kleinventilatoren zur Geräuschreduzierung*. In: VDI Berichte 1922 (2006), **2006**

[13] T. Carolus – *Ventilatoren. Aerodynamischer Entwurf, Schallvorhersage, Konstruktion*. Book, Vieweg+Teubner Verlag, **2003**